An investigation of propagation characteristics of the gravity waves at Shigaraki using the imaging data of four nightglow emissions

D. Gobbi, R. Maekawa, T. Nakamura, T. Tsuda, K. Shiokawa

Radio Atmospheric Science Center, Kyoto University

Solar-Terrestrial Environment Laboratory, Nagoya University

ABSTRACT

A collaborative MU radar and imaging observations of nightglow emissions over Shigaraki (35^{o}N, 136^{o}E), Japan, was carried out between January and March as part of the Planetary Scale Mesopause Observing System (PSMOS) campaign to investigate the horizontal structure of gravity waves around the mesopause region. The horizontal wavenumbers and apparent frequencies of quasi-monochromatic wave events of short periods (< 1 hour) and small-scale (10 ~ 80 km) were determined from four nightglow emission layers, OI 557.7 nm (~ 96 km), O_2 A (0-1) band (~ 94 km), Na 589.3 nm (~ 90 km) and NIR OH bands (~ 87 km). This information was combined with simultaneous MU radar wind and SATI temperature measurements at the same height range to derive the intrinsic wave parameters for these events. Using the background structure information, the propagating characteristics such as wave ducting, evanescence and vertical propagation as internal modes was investigated. The study revealed a significant fraction of occurrence of non-propagation events with approximately 60% of all events. These results suggest that the small-scale gravity waves are highly susceptible to the variations of the mean flow and that the ducted effects are relatively common in the upper mesosphere.

INTRODUCTION

The imaging techniques using a high-resolution CCD cameras have enabled us to study and visualize the gravity waves near the mesopause region especially for the short period (< 1 hour) and horizontal small-scale (10 ~ 80 km) gravity waves (e.g., Nakamura *et al.,* 1999, Taylor *et al*., 1997; Swenson *et al*., 1995), which are important in transporting momentum upward into the lower thermosphere (e.g., Fritts, 1984). The imaging data provide information about the direction of propagation, horizontal wavelength and apparent phase velocity of each wave event detected in the emission layer. This set of parameters together with joints measures of the mean winds and thermal structure permitts to inferr the intrinsic characteristics of the vertical wave propagation. Recently, a comparative study of nightglow images and MF radar data (Isler *et al*., 1997) has pointed out the possibility that significant part of these small-scale gravity waves observed by imagers could be ducted or evanescent. Thus, a detailed observation of these gravity waves and their propagating characteristics is of our great interest in order to understand the dynamical role of the gravity waves near the mesopause region.

EXPERIMENTAL DATA

The observations reported in this work were obtained at the MU radar site in Shigaraki (35^{o}N, 136^{o}E), Japan, in January 21 to February 4, 1998 and February 18 to March 5, 1998, as part of the Planetary Scale Mesopause Observing System (PSMOS-98) campaign. The primary data presented on were obtained from four all-sky CCD cameras (three from Nagoya University and one from the Kyoto University) to detecting the fluctuations in nightglow emissions. The CCD cameras are discussed in some details by Shiokawa *et al.* (1999). The additional data used in this paper refers on: (1) the MU radar (as a meteor radar) to assessing the background wind and the fluctuations of the relative temperature; (2) the Spectral Airglow Temperature Imager (SATI) to determining the reference temperature profile. The general operation of the MU radar are discussed by Tsuda *et al.* (1990), while Tsutsumi *et al.* (1994) describe the derivation of the relative temperature around the mesopause. In addition, details about the SATI technique are extensively considered by Wiens *et al.* (1997).

The CCD cameras passband filters, onto a back-illuminated 512 $\times$ 512 pixel array (Hamamatsu C4880). The nominal integration time per filter is 110 s, except for NIR OH image that is 20 s. Therefore, there were simultaneous images every 2 min approximately. Considering a monochromatic wave motion, this means a limiting Nyquist period of 4 min. In this way, enable us to estimate the wave periods in the order of the Brunt-Väisälä periods (around 5 min at 87 km). The field of view is about 768 $\times$ 768 km^2 by assuming the characteristic heights of the nightglow emission layers.

The presence of the background wind may letting the apparent wave period differ largely from the intrinsic period of the wave, due the Doppler shifting by the mean wind. For this analysis, the wind database available refers to coincident

operation of the MU radar in the metor mode with the optical observations period of the PSMOS campaign. The nominal wind evaluation corresponds to 30 min time intervals and 1 km vertical resolution, between 78 and 100 km (nightime). However, the effective altitude range of the wind data available for this study is ~ 82–97 km, because of some missing data (low meteor echo rate). Hasebe *et al.* (1997) estimated that the statistical significance of the wind field is 6 m/s in 90 km of altitude.

ANALYSIS AND RESULTS

The optical observations in the first part of the PSMOS campaign were made during two consecutive new moon periods: 21 January to 03 February and 21 February to 03 March. A result of this inspection is shown in the Figure 1, which draws the histogram of gravity wave event and "clear sky" (no evidence of clear wave signatures) observing time, within the all-sky field specially for the OI nightglow emission, in view of this one presented images with the greatest contrast compared to the others emissions. Aproximately, 90 hours of useable data were recorded on 15 nights, where ~$1/3$ of this amount exhibits wave activity. This frequency varies to the others emissions, because of the lower contrast or sometimes lack of contrast in the images, suggesting that the effects due to the mean flow played an important role during this observation period.

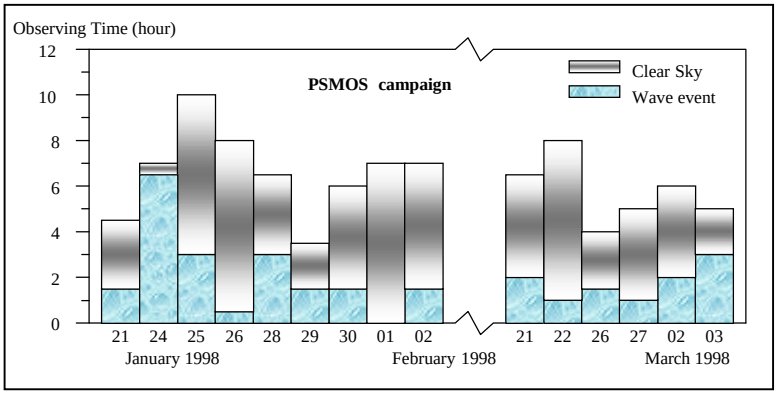

Fig. 1. Frequency of occurrence of **wave event** and **"clear sky"** observing hours, within the all-sky field for the OI emission.

Gravity Wave-Mean Flow Interaction: Propagation Modes. The differential equation governing the propagation of the gravity waves in a horizontally stratified and windy atmosphere, under the Boussinesq form, and assuming periodic solutions in time and in the horizontal direction (monochromatic plane waves), can be given by (e.g., Gossard and Hooke, 1975),

$$\frac{\partial^2 w'}{\partial z^2} + \left[\frac{N_o^2}{(u_o - c)^2} - \frac{\partial^2 u_o / \partial z^2}{(u_o - c)} - k_h^2 \right] w' = 0, \qquad (1)$$

also known as Taylor-Goldstein equation, where w' is the vertical velocity perturbation, N_o is the Brunt-Väisälä frequency, u_o is the background wind speed (time-averaged) along the wave direction, c and k_h are the gravity wave parameters: phase velocity and horizontal wavenumber, respectively.

The equation (1) encloses the important special cases of the gravity wave propagation (such as the critical level problem) and is the starting point for determining the effects of wind shear and buoyancy frequency variations on the path of the gravity wave through the upper mesosphere. A conventional approach for analyzing such cases is to use an approximate theory, called the WKB method (e.g., Andrews *et al*., 1987), with the vertical wave number defined from the equation (1) by

$$m^2 = \frac{N_o^2}{(u_o - c)^2} - \frac{\partial^2 u_o / \partial z^2}{(u_o - c)} - k_h^2. \qquad (2)$$

The validity of the WKB method may be only justified since that the $u_o(z)$ and $N_o^2(z)$ do not present rapid variations with height (Lindzen, 1981).

Equation (2) presents solutions for freely propagating waves on the condition $m^2(z) > 0$; in case of $m^2(z) < 0$, induced by the variations in $u_o(z)$ or $N_o^2(z)$ or both, simultaneously, exists an evanescence region and the gravity wave is not allowed freely propagate, producing reflection of wave energy. The ducted wave structure to take place when $m^2(z) > 0$ in a determined height interval and bounded by $m^2(z) < 0$. This process limits the vertical propagation of the gravity waves and restricts their tranports of energy and momentum to a confine range of heights.

Analysis of the Wave Parameters. The Table 1 summarizes the results obtained from the 15 nights during the PSMOS campaign. The wave events are classified in chronological sort and labeled by a sequence of numbers. The total number of events identified was 23 that only a fraction of these events (~50%) were detected in all four emission layers. Futhermore, the table lists the calculated horizontal parameters (azimuth, wavelength, apparent period and phase velocity), the background velocity in the wave azimuth (the range of values) and the mean Brunt Väisälä period (the range of values) for each identifiable event. In this way, with the use of the equation (2), were estimated the vertical wavenumber squared profiles (m^2) in each case.

Table 1. List of the Horizontal Wave Parameters (from the image data) and the intrinsic wave parameter (from MU radar)

Wave Event	Date yy.mm.dd	*Emission layer*	*Azimuth* (°N)	λ_h (km)	τ (min)	c (m/s)	$u_o(z)$ (m/s)	$\lambda_z(z)$ (km)	*Freely* Propagate	Evanescent / Ducted
1	98.01.21	OH,Na,O_2,OI	110	19 ± 1	9 ± 1	35 ± 3	0 – 20	6 – 18	×	
2	98.01.24	OH,O_2,OI	304	44 ± 2	13 ± 2	56 ± 5	(-70) – 0			×
3	98.01.24	OH,O_2,OI	53	26 ± 1	9 ± 2	48 ± 6	0 – 80	1 – 30	×	
4	98.01.25	O_2,OI	165	28 ± 1	15 ± 2	31 ± 2	(-77) – 20			×
5	98.01.25	OH,O_2,OI	40	47 ± 2	8 ± 1	98 ± 7	11 – 98	1 – 33	×	
6	98.01.28	OH,Na,O_2,OI	225	42 ± 2	10 ± 3	70 ± 10	(-97) – (-20)			×
7	98.01.28	OH,O_2,OI	204	17 ± 1	10 ± 1	28 ± 2	(-98) – (-26)			×
8	98.01.29	OH,Na,O_2,OI	218	28 ± 2	14 ± 2	33 ± 3	(-42) – (-4)			×
9	98.01.29	O_2,OI	150	12 ± 1	8 ± 3	25 ± 5	(-29) – 40			×
10	98.01.30	OH,Na,O_2,OI	239	50 ± 3	15 ± 3	56 ± 6	(-47) – 0	39 – 76	×	
11	98.02.02	OH,Na,O_2,OI	210	15 ± 1	11 ± 2	23 ± 2	(-28) – 60			×
12	98.02.21	OH,Na,O_2,OI	230	42 ± 3	20 ± 4	35 ± 4	–			
13	98.02.21	OH,O_2,OI	130	12 ± 1	7 ± 2	29 ± 4	–			
14	98.02.22	OH,Na,O_2,OI	138	28 ± 2	9 ± 2	52 ± 6	–			
15	98.02.26	OH,Na,O_2,OI	204	24 ± 2	16 ± 2	25 ± 2	–			
16	98.02.26	O_2,OI	298	40 ± 2	10 ± 2	67 ± 7	–			
17	98.02.27	OH,Na,O_2,OI	190	15 ± 1	9 ± 1	28 ± 2	–			
18	98.02.27	OH,Na,O_2,OI	161	30 ± 2	7 ± 1	72 ± 5	–			
19	98.03.02	OH,OI	42	42 ± 3	13 ± 1	54 ± 3	0 – 50			×
20	98.03.02	OH,O_2,OI	60	24 ± 1	9 ± 1	45 ± 3	0 – 53	2 – 33	×	
21	98.03.03	O_2,OI	137	15 ± 1	8 ± 1	31 ± 2	(-13) – 50			×
22	98.03.03	OH,Na,O_2,OI	68	35 ± 1	13 ± 1	45 ± 2	(-21) – 40	4 – 11	×	
23	98.03.03	OH,Na,O_2,OI	123	46 ± 3	9 ± 1	85 ± 5	(-18) – 44	23 – 40	×	

Using the scheme provided by the equation (2) (section 3.2) to classify the vertical motion as freely propagating, evanescent or ducted wave modes, was studied 16 events over the 83 – 97 km range altitudes. However, sometimes was difficult to distinguish between the non-propagating modes: ducted or evanescent wave, due basically to high relative uncertainties on the border of the $m^2(z)$ and to limited range of the background structure. For this reason, the

Table 1 lists the events arranged as propagating or non-propagating modes. It reveals a significant fraction of occurrence of non-propagation events with ~ 60% of all events. A similar result was obtained by Isler *et al.* (1997) that analysed 36 quasi-monochromatic wave events inffering that ~ 75% of their presented non-propagating behaviour. This characteristics is associated with the high variability in time of the mean flow structure for these small scales waves, producing ducts or evanescence region through the vertical motion.

The Figure 2 shows a histogram plot for the number of freely propagating events and the number of non-propagating events as a function of wavelength bin. As can be seen, the smaller-scale gravity waves are more likely to be ducted or evanescent than larger-scale waves, in agreement with Doppler ducting theory (k^2 is large).

CONCLUSIONS

Simultaneous mean winds and high-resolution imaging measurements were made from the MU radar site in Shigaraki (35°N, 136°E), Japan, between January and March, 1999, as part of PSMOS campaign. A study of 16 quasi-monochromatic events has revelead a significant fraction of them (up to 60 %) to be occurrence of evanescent or ducted gravity wave. Our present results also show that the smaller-scale waves are more likely to be ducted than larger-scale waves, in agreement with Doppler ducting theory. The predominance of non-propagating waves has much significance for observational and modeling studies that assume gravity waves to be freely propagating.

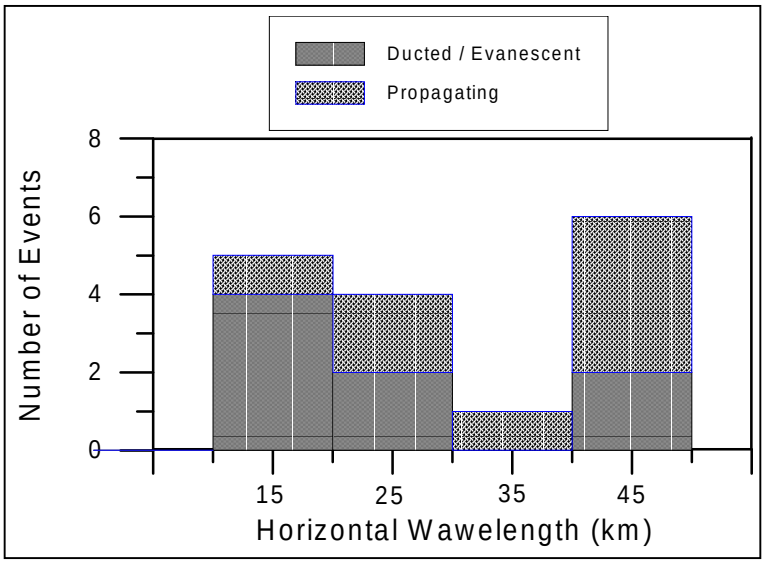

Fig. 2. Histogram plot showing the number of propagating events and the number of non-propagating events as a function of wavelength bin.

REFERENCES

Andrews, D. G., J. R. Holton, and C. B. Leovy, Middle Atmosphere Dynamics, Academic Press, Orlando, 1987.

Fritts, D. C., Gravity wave saturation in the middle atmosphere: A review of theory and observations, Rev. Geophys., 2, 275-307, 1984.

Gossard, E. E., and W. H. Hooke, Waves in the Atmosphere, Elsevier, New York, 1975.

Hasebe, F., T. Tsuda, T. Nakamura, and M. D. Burrage, Validation of HRDI MLT winds with meteor radars, Ann. Geophysicae, 15, 1142-1157, 1997.

Hech, J. H., R. L. Walterscheid, and N. N. Ross, First measurements of the two-dimensional horizontal wave number spectrum from CCD images of the nightglow, J. Geophys. Res., 99, 11499-11460, 1994.

Isler, J. R., M. J. Taylor, and D. C. Fritts, Observational evidence of wave ducting and evanescence in the mesosphere, J. Geophys. Res., 102, 26301-26313, 1997.

Lindzen, R. S. Turbulence and stress owing to gravity wave and tidal breakdown, J. Geophys. Res., 86, 9707-9714, 1981.

Nakamura, T., A. Higashikawa, T. Tsuda, and Y. Matsushita A long term observation of gravity wave structures in OH airglow with a CCD imager at Shigaraki, Earth Planets Space, in press.

Shiokawa, K., Y. Katoh, M. Satoh, M. K. Ejiri, T. Ogawa, T. Nakamura, T. Tsuda, and R. H. Wiens, Development of Optical mesosphere Thermosphere Imagers (OMTI), Earth Planets Space, in press.

Swenson, G. R., M. J. Taylor, P. J. Espy, C. Gardner, and X. Tao, ALOHA-93 measurements of intrinsic AGW characteristics using airbore airglow imager and groundbased Na wind temperature lidar, Geophys. Res. Lett., 22, 2841-2844, 1995.

Taylor, M. J., W. R. Pendleton Jr., S. Clark, H. Takahashi, D. Gobbi, and R. A. Goldberg, Image measurements of short-period gravity waves at equatorial latitudes, J. Geophys. Res., 102, 26283-26299, 1997.

Tsuda, T., S. kato, T. Yokoi, T. Inoue, M. Yamamoto, T. E. VanZandt, S. Fukao, and T. Sato, Gravity waves in the mesophere observed with the MU radar, Radio Sci., 26, 1005-1018, 1990.

Tsutsumi, M., T. Tsuda, T. Nakamura, and S. Fukao, Temperature fluctuations near the mesopause inferred form meteor observations with the middle and upper atmosphere radar, Radio Sci., 29, 599-610, 1994.

Wiens, R. H., A. Moise, S. Brown, S. Sargoytchev, R. N. Petersen, G. G. Shepherd, M. J. Lopez-Gonzales, J. J. Lopez-Moreno, and R. Rodrigo, SATI: A spectral airglow temperature imager, Adv. Space Sci., 19, 677-680, 1997.

ACKNOWLEDGMENTS

Support for the optical measurements was provided by the collaborative program (PSMOS campaign) between the Solar-Terrestrial Environment Laboratory (Nagoya University) and the Radio Atmospheric Science Center (RASC / Kyoto University). Support for the radar measurements as part of the PSMOS campaign was provided by RASC. One of us (Delano Gobbi) thanks the CNPQ (Brasil) for scholarship support under contract 200747/97-5.